

1 **Predicting soil and plant water status dynamic in olive orchards under different irrigation**  
2 **systems with Hydrus-2D: Model performance and scenario analysis**

3

4 **Dario Autovino<sup>1</sup>, Giovanni Rallo<sup>2</sup>, Giuseppe Provenzano<sup>3</sup>**

5 <sup>1</sup> PhD, Dipartimento Scienze Agrarie, Alimentari e Forestali, Università degli Studi di  
6 Palermo, Viale delle Scienze 12, 90128 Palermo, Italy. Email: [dario.autovino@unipa.it](mailto:dario.autovino@unipa.it)

7 <sup>2</sup> PhD, Researcher. Department of Agriculture, Food and Environment (DAFE), Università di  
8 Pisa, Via del Borghetto 80, 56124 Pisa, Italy. Email: [giovanni.rallo@unipi.it](mailto:giovanni.rallo@unipi.it)

9 <sup>3</sup> PhD, Professor. Dipartimento Scienze Agrarie, Alimentari e Forestali, Università degli Studi  
10 di Palermo, Viale delle Scienze 12, 90128 Palermo, Italy. Email:  
11 [giuseppe.provenzano@unipa.it](mailto:giuseppe.provenzano@unipa.it)

12

13 **Abstract**

14 The paper analyzes the performance of Hydrus-2D model to simulate the dynamic of soil water  
15 contents and transpiration fluxes in an olive orchard in which two different irrigation systems  
16 were used in 2011 and 2012. Secondly, the relationship between midday stem water potential,  
17 *MSWP*, and relative transpiration (ratio between simulated actual and maximum crop  
18 transpiration),  $K_s$ , was identified with the aim to use the model for crop water status predictions.  
19 Model validation was carried out based on the comparison between simulated and measured  
20 soil water contents at different points of soil domain, as well as between simulated root water  
21 uptake and transpiration fluxes measured with sap flow sensors. The latter were examined under  
22 the hypothesis to neglect tree capacitance and hence the contribute of water stored in leaves,  
23 branches and trunk of the tree to transpiration fluxes. Finally, a scenario analysis was carried

24 out for irrigation management purposes, by considering the level of crop water stress achieved  
25 in the different phases of the vegetative growth.

26 Data used to parametrize the model were acquired in a commercial farm located in South-West  
27 of Sicily, in an area where olive represents the main orchard crop. Preliminary experiments  
28 allowed parametrizing soil hydraulic and root density distribution functions in the soil domain  
29 of a single tree. During the first year irrigation water was applied with a drip lateral placed along  
30 the plant row, whereas in the second year by means of a network of emitters laid on the soil and  
31 covering the entire surface dominated by a plant. Soil water contents at different depths and  
32 distances from the plant row were monitored by a Frequency Domain Reflectometry (*FDR*)  
33 sensor, whereas sap flow velocity by Thermal Dissipation Probes (*TDP*). The latter then  
34 allowed estimating transpiration fluxes based on the measured conducting sapwood. Moreover,  
35 in 2011 crop water status was monitored according to *MSWP* measured roughly weekly, with a  
36 Scholander chamber.

37 The results evidenced that active roots ( $d < 2.0$  mm) were mainly detected along the tree row  
38 where is installed the drip irrigation pipe, with concentrations that tended to decrease at  
39 increasing depth and with the distance from the plant row. It was demonstrated that Hydrus-2D  
40 model is generally able to reproduce the trends of measured soil water contents at different  
41 distances and depths from the plant row with *RMSE* equal to  $0.04 \text{ cm}^3 \text{ cm}^{-3}$  in 2011 and  $0.09$   
42  $\text{cm}^3 \text{ cm}^{-3}$  in 2012, because of the inadequate schematization of the root system, that could have  
43 changed according to the different irrigation system. Moreover, the model was also suitable to  
44 estimate actual transpiration with *RMSE* values, in the two years, of 0.09 and 0.05 mm. It was  
45 also observed that measured *MSWPs* are linearly correlated to the ratio between actual and  
46 maximum transpiration; under the examined conditions in fact, reductions of *MSWP* from -1.5  
47 MPa to -3.1 MPa determined a decline of actual transpiration from about 86% to 50% of

48 maximum. Finally, the performed scenario analysis evidenced the potential of the model to  
49 identify crop water status during the different stages of crop growth, that can be used to identify  
50 irrigation strategies aimed to cope with water scarcity.

51

52 **Key-words**

53 Hydrus-2D; Olive tree; Actual evapotranspiration; Water stress; Midday Stem Water Potential;

## 54 **Introduction**

55 In several regions of the world, the scarcity of freshwater represents one of the most important  
56 environmental concerns due to agricultural intensification associated to the increasing  
57 population and rapid economic growth. Moreover, the climate change scenario may exacerbate  
58 the problem, creating new drought-prone areas or increasing those affected by severe aridity  
59 (Provenzano and Rodriguez-Sinobas, 2014). Compared to the traditional surface or sprinkler  
60 irrigation, well-designed drip systems, characterized by high field distribution uniformity, can  
61 allow enhancing irrigation efficiency (Autovino et al., 2016; Martì et al., 2010) however, there  
62 are many other management factors that may affect the performance of these systems (Egea et  
63 al., 2016). Further findings in implementation and testing of water-saving strategies associated  
64 to irrigation scheduling are therefore desirable, even to assure the appropriate feedback between  
65 research and practice (Provenzano et al., 2014). Researches related to the optimization of  
66 irrigation for olive trees have demonstrated that slight or moderate crop water stress in specific  
67 phenological stages can contribute to increase crop productivity and water use efficiency  
68 (Tognetti et al., 2004).

69 When applying water-saving strategies it is necessary the precise control of irrigation by  
70 monitoring specific indicators related to soil and plant water status (soil matric potential, leaf  
71 or stem water potential, trunk diameter variations, relative transpiration) aimed to identify  
72 proper irrigation timing and depth (Rallo et al., 2014a), so to prevent severe stress conditions  
73 and unreasonable water consumes. As stated by Kramer (1969), “the status of water in the plant  
74 represents an integration of the atmospheric demand, soil water potential, rooting density and  
75 distribution, as well as other plant characteristics”. For these reasons, the monitoring of plant  
76 water status should be preferred to that related to the soil water status or to the climatic  
77 variables.

78 Leaf or stem water potential, measured at predawn or midday, are in fact considered among the  
79 most reliable indicators of crop water status, whereas sap flow sensors are suitable to quantify  
80 the plant transpiration fluxes. In remote modality, crop reflectance spectroscopy or thermal  
81 images are also considered valid tools to detect crop water status at various spatial scales  
82 (Gamon and Qiu, 1999; Rallo et al., 2014b). In alternative, measurements of soil water contents  
83 have been quite often preferred because of their simplicity even though, under trickle irrigation,  
84 the high water gradients around the emission points makes it difficult to identify the spot in  
85 which the soil water content representative of the root volume has to be detected. However,  
86 despite crop-base measurements represent the most effective way to schedule irrigation because  
87 integrates environmental effects and potentially very sensitive, these don't indicate how much  
88 water to apply. Moreover, calibration procedures are required to determine control thresholds  
89 (Jones, 2004).

90 For these reasons easy-to-use tools, such as software packages simulating water transfer in the  
91 soil-plant-atmosphere (SPA) continuum, are often used for indirect evaluations of soil and crop  
92 water status and to estimate indicators related to water stress (Minacapilli et al., 2009;  
93 Cammalleri et al., 2013; Rallo et al., 2017). Several agro-hydrological models have been  
94 implemented and used to explain the water exchange processes occurring in the SPA continuum  
95 (Rallo and al., 2012). The complexity of the system not only derives from the high number of  
96 variables to be defined, but also from internal self-regulation phenomena occurring between the  
97 system components (Rallo et al., 2010).

98 Hydrus-2D package (Šimůnek et al., 1999) allows simulating water, heat and multiple solute  
99 transfer in variably saturated porous media. Since its implementation, the model been  
100 extensively applied as summarized in the review of Šimůnek et al., (2016), in which the  
101 capabilities and the major applications allowed by the different versions were presented and

102 discussed. Despite several applications on horticultural crops and under different climates have  
103 been provided the model validation with reference to soil water content (Mguidiche et al., 2015;  
104 Egea et al., 2016; Ghazouani et al., 2016) only a few have accounted for the impact of irrigation  
105 strategies on water plant uptake, actual crop transpiration or crop yield (Mailhol et al., 2011).  
106 Phogat et al. (2013) used the model to evaluate daily fluctuations of water fluxes of almond  
107 trees under different irrigation management. These authors evidenced the good performance of  
108 the model to reproduce the spatial and temporal water dynamic in the soil domain, also  
109 observing that the model simulates daily values of root water uptake well responding to the  
110 fluctuations of evapotranspiration demand; however, according to their results, the magnitude  
111 of simulated root water uptake resulted generally greater than the corresponding measured with  
112 sap-flow sensors.

113 The main objective of the paper was to assess the performance of Hydrus-2D model to predict  
114 soil water contents and transpiration fluxes in an olive orchard maintained under two different  
115 irrigation systems. After validating the model and assessing the relationship between midday  
116 stem water potential (*MSWP*) and the ratio between simulated actual and maximum crop  
117 transpiration, a scenario analysis was carried out in order to verify the possibility to decrease  
118 seasonal irrigation-water requirement by controlling the levels of water stress achieved in the  
119 different phases of the vegetative crop growth.

120

## 121 **Background of Hydrus-2D model**

122 Hydrus-2D model (Simunek et al., 1999) allows simulating water flow, heat and solute transport  
123 in two-dimensional variably-saturated flow domain. Furthermore, the model allows estimations  
124 of root water uptake, according to which the spatial distribution of soil water content is  
125 evaluated.

126 A modified form of Richards equation is used to describe water movement in the soil, under  
 127 the hypotheses to neglect the air phase and the thermal gradients in the soil (Celia et al., 1990):

$$\frac{\partial \theta}{\partial t} = \frac{\partial}{\partial x} \left[ K(h) \frac{\partial h}{\partial x} \right] + \frac{\partial}{\partial z} \left[ K(h) \frac{\partial h}{\partial z} + K(h) \right] - S(h) \quad (1)$$

128 where  $\theta$  [ $L^3 L^{-3}$ ] is volumetric soil water content,  $t$  [T] is time,  $h$  [L] is soil matric potential,  
 129  $K(h)$  [ $L T^{-1}$ ] is unsaturated soil hydraulic conductivity,  $x$  [L] and  $z$  [L] are the horizontal and  
 130 vertical (positive upwards) spatial coordinates and finally,  $S(h)$  [ $T^{-1}$ ] is a sink term representing  
 131 the volume of water extracted by plant roots from the unit soil volume and in a time unit.  
 132 Equation (1) is solved by using the Galerkin-type finite element method applied to a network  
 133 of triangular elements (mesh).

134 The model requires the knowledge of the soil water retention curve,  $\theta(h)$  and the hydraulic  
 135 conductivity function,  $K(h)$ , that can be mathematically described by means of the van  
 136 Genuchten-Mualem model (Mualem, 1976; van Genuchten, 1980):

$$\theta(h) = \theta_r + \frac{\theta_s - \theta_r}{[1 + (ah)^n]^m} \quad h < 0 \quad (2)$$

$$\theta(h) = \theta_s \quad h \geq 0 \quad (3)$$

$$K(h) = K_s S_e^l \left[ 1 - (1 - S_e^{1/m})^m \right]^2 \quad (4)$$

137 where  $\theta_s$  [ $L^3 L^{-3}$ ] and  $\theta_r$  [ $L^3 L^{-3}$ ] are saturated and residual soil water content,  $m$ ,  $n$  and  $a$  are  
 138 function shape parameters, with  $m = 1 - 1/n$ ,  $K_s$  [ $L T^{-1}$ ] is saturated hydraulic conductivity,  $l$   
 139 is the pore connectivity parameter and  $S_e$  is relative saturation, defined as:

$$S_e = \frac{\theta - \theta_r}{\theta_s - \theta_r} \quad (5)$$

140 In the absence of osmotic stress, the actual rate of root water uptake,  $S(h)$ , in any point of  
 141 simulation domain is computed according to the Feddes model (Feddes et al. 1978), that

142 assumes that  $S(h)$  is proportional to the maximum root uptake rate occurring when water is not  
 143 limiting plant transpiration,  $S_m$  [ $T^{-1}$ ]:

$$S(h) = \alpha(h) S_m \quad (6)$$

144 where the water stress response function,  $\alpha(h)$  [-], locally depends on soil matric potential.

145 To describe the water stress response function, van Genuchten (1987) suggested the following  
 146 sigmoid function (S-shape), valid in the absence of osmotic stress:

$$\alpha(h) = \frac{1}{1 + \left(\frac{h}{h_{50}}\right)^p} \quad (7)$$

147 The model assumes that the reductions of water uptake depends on i) the soil matric potential  
 148 for which the ratio between actual and maximum crop transpiration is equal to 0.5,  $h_{50}$  [L], and  
 149 on ii) a dimensionless parameter,  $p$  [-], whose value is influenced by soil, crop and climate  
 150 conditions (Homaei, 1999).

151 Under non-uniform root distribution, the spatial variation of maximum root extraction,  $S_m$ , is  
 152 expressed as:

$$S_m = \beta(x, z) L_t T_m \quad (8)$$

153 where  $\beta(x, z)$  [ $L^{-2}$ ] is a normalized distribution of maximum root water uptake over a soil volume  
 154 of arbitrary shape (Vogel, 1987),  $L_t$  [cm] is the width of soil surface associated with the  
 155 transpiration process and  $T_m$  [ $L T^{-1}$ ] is the maximum transpiration.

156 The actual water uptake distribution in any point of the simulation domain is obtained by  
 157 introducing eq. (8) into eq. (6):

$$S(h, x, z) = \alpha(h, x, z) \beta(x, z) L_t T_m \quad (9)$$

158 By integrating eq. (9) in the region occupied by roots it is possible to obtain the total actual root  
 159 water uptake that, by neglecting the tree capacitance, can be assumed corresponding to actual  
 160 plant transpiration.



161 In Hydrus-2D, the normalized  $\beta(x,z)$  function is implemented according to the model proposed  
162 by Vrugt et al. (2001):

$$\beta(x, z) = \left[ \left( 1 - \frac{z}{Z_m} \right) \right] \left[ \left( 1 - \frac{x}{X_m} \right) \right] e^{-\left( \frac{p_z}{Z_m} |z^* - z| + \frac{p_x}{X_m} |x^* - x| \right)} \quad (10)$$

163 where  $Z_m$  [L] and  $X_m$  [L] are the maximum rooting lengths in the  $z$  and  $x$  directions,  $z^*$  [L] and  
164  $x^*$  [L] define the location of the maximum root water uptake in vertical ( $z$ ) and horizontal ( $x$ )  
165 directions and finally,  $p_z$  [-] and  $p_x$  [-] are empirical coefficients.

166

## 167 **Materials and Methods**

### 168 *Study area and data collection*

169 Experiment was conducted at “Tenute Rocchetta”, a commercial farm (*Olea europaea* L., cv.  
170 *Nocellara del Belice*) located in South-West of Sicily, Italy (37.6494 N, 12.8492, E, 123 m  
171 a.s.l.) during two irrigation seasons (2011 and 2012). The farm, specialized in the production  
172 of oil and table olives, is located in a quite flat area with a rather homogeneous silty-clay-loam  
173 soil texture. Climate is typically Mediterranean with precipitation concentrated in fall and  
174 winter and a dry season lasting 4-5 months, from late spring to late summer. A standard weather  
175 station by the Sicilian Agrometeorological Information Service (SIAS) located 500 m apart the  
176 experimental site, allowed acquiring daily precipitations, as well as the climate variables to  
177 estimate reference evapotranspiration,  $ET_0$ , with the Penman Monteith equation (Allen et al.,  
178 1998), whose validity for the experimental site has been previously assessed (Minacapilli et al.,  
179 2016).

180 The orchard was planted about 25 year ago, with rows roughly oriented along the East-West  
181 direction and plant spaced 5.0 m within rows and 8.0 m between rows. Two undisturbed  
182 cylindrical soil samples, 8.5 cm diameter and 5.0 cm height, were collected at different depths

183 (0-15, 15-45, 50-70 and 80-100 cm) to determine soil water retention curve and hydraulic  
184 conductivity function. Hanging water column apparatus (Burke et al., 1986) was used for soil  
185 matric potential ranging between -0.05 m and -1.50 m, whereas the pressure plate apparatus  
186 (Dane and Hopman, 2002) for soil matric potential values from -3.37 to -153.0 m. Soil water  
187 conductivity corresponding to matric potentials close to saturation were determined by tension  
188 disc infiltrometer (Logsdon et al., 1993) and the Beerkan Estimation of Soil Transfer (BEST)  
189 method (Bagarello et al., 2011).

190 During the first year (2011) investigated trees were irrigated by a single drip lateral per plant  
191 row, with four 8.0 l/h emitters per plant, installed at both sides of each trunk at distances of 0.50  
192 m and 1.50 m (fig. 1a). In 2012, in order to reproduce a different irrigation system, water was  
193 distributed over the entire soil surface dominated by a plant, with 8.0 l/h emitters installed  
194 according to a square grid spaced 50 cm, and positioned on the ground (fig. 1b). In both years,  
195 phase I of vegetative growth lasted around 10 of July, the end of the pit hardening stage around  
196 20 of August, whereas phase II of vegetative growth continued till the end of October. Irrigation  
197 events were scheduled from mid of July to the end of August, whereas all the other management  
198 and fertilization options followed the ordinary practices used by the farmer.

199 Soil water contents were monitored by Frequency Domain Reflectometry (FDR) downhole  
200 sensor (Diviner 2000, Sentek), after evaluating the site-specific calibration equation (Rallo and  
201 Provenzano, 2014; Provenzano et al., 2015). Sixteen 120 cm long access tubes (P1-P16) were  
202 installed in a quarter of a tree, as indicated in fig. 1a,b.

203 In order to detect the spatial distribution of active roots from soil surface to 105 cm depth, seven  
204 undisturbed cylindrical soil cores, 5 cm diameter and 15 cm height, were collected during the  
205 installation of each *FDR* access tube, for a total of 112 samples. Root extraction was carried out  
206 by following a standard procedure of wash and filtration (Newman, 1966). In each sample, the

207 total length of roots with diameter lower than 2 mm was scanned and measured with Image-Pro  
208 Plus 6.0 software (Media Cybernetics, Silver Spring, US). Values of normalized Root Length  
209 Density (*RLD*) were finally determined and assumed as the length of active roots in each soil  
210 unit.

211 In order to monitor sap flow velocity,  $v$  [ $\text{cm min}^{-1}$ ], two pairs of thermal dissipation probes,  
212 *TDP*, (Granier, 1987) were installed in an olive tree at height of about 40 cm from the ground  
213 in the convex and concave side of the trunk, which was then wrapped in reflective insulation.  
214 The probes were connected to a Campbell CR1000 (Campbell Scientific Inc., Logan, Utah)  
215 datalogger, programmed to acquire at hourly time-step. Sap flow velocity [ $\text{cm min}^{-1}$ ] was  
216 obtained by combining the difference of temperature between heated and un-heated needle with  
217 the corresponding difference registered at night (absence of flux). Sap fluxes,  $q$  [ $\text{cm}^3 \text{min}^{-1}$ ],  
218 were then evaluated by multiplying sap flow velocity to the cross-area,  $S$  [ $\text{cm}^2$ ], of the  
219 conducting sapwood, measured by colorimetric method on trunk samples extracted with the  
220 Pressler gimlet (Cammalleri et al., 2013). Hourly fluxes were then aggregated at daily time-step  
221 and assumed equivalent to plant transpiration, under the hypothesis to neglect tree capacitance.  
222 Crop water status was monitored based on Midday Stem Water Potential (*MSWP*), measured  
223 with Scholander pressure chamber (Scholander et al., 1965) by following Turner and Jarvis  
224 (1982) protocol. Two measurements of *MSWP* [MPa] were carried out roughly every week  
225 from June 27 to September 18, 2011, on non-transpiring stems collected in the same trees where  
226 sap flow sensors were installed. Measurements were carried out at least 30 minutes after  
227 insulating the stems with aluminum foil faced bags.

228

229 ***Parametrization of Hydrus-2D model and scenario analysis***

230 Hydrus-2D model validation was carried out by considering both the described drip distribution  
231 systems. A two-dimensional simulation domain perpendicular to the drip pipe, 150 cm deep  
232 and 400 cm wide, was used to schematize the soil volume around a single tree as shown in fig.  
233 1a,b. Simulations were run from January, 1, 2011 to December 31, 2012, with daily time step  
234 (731 days). For both years, the flow domain was discretized by unstructured mesh with a total  
235 of 1134 nodes and 2147 finite triangular elements, whose dimensions were assumed smaller at  
236 the top layer, where the highest hydraulic gradients occurred. In 2011, drip irrigation was  
237 simulated by an infinite line source perpendicular to the flow domain, as previously adopted by  
238 other authors (Skaggs et al., 2010; Phogat et al., 2013). This assumption is consistent with the  
239 long lasting irrigation, during which the overlapping of wetted bulbs was observed in the field.  
240 The atmospheric boundary condition was set at the top edge of the simulation domain, with the  
241 exception of the three nodes (12.5 cm) placed below the emitter, in which a time-variable  
242 boundary condition was considered. By assuming that in 2011 the area wetted by emitters is 25  
243 cm wide and 500 cm long (12,500 cm<sup>2</sup>) and considering the volume distributed during each  
244 irrigation event equal to 400 dm<sup>3</sup> d<sup>-1</sup>, a flux  $q=32$  cm d<sup>-1</sup>, was obtained. In 2012, based on the  
245 adopted distributed drip system, watering was simulated as a daily event, whose height was  
246 obtained by dividing the irrigation volume to the surface dominated by a single plant. In both  
247 the considered years, the absence of flux was assumed along the lateral boundary surfaces and  
248 free drainage at the bottom of soil profile.

249 The maximum daily crop transpiration,  $T_m$ , and soil evaporation,  $E_m$ , used to define the time-  
250 variable atmospheric boundary condition, were estimated from  $ET_0$  values by following the  
251 dual crop coefficient approach (Allen et al., 1998), as:

$$252 \quad T_m = K_{cb} ET_0 \quad (11)$$

$$253 \quad E_m = K_e ET_0 \quad (12)$$

254 in which  $K_{cb}$  is the basal crop coefficient evaluated on the basis of the canopy fraction cover  
255 and the tree height (Allen and Pereira, 2009) and  $K_e$  is the coefficient of soil evaporation, that  
256 was set equal to 0.1.

257 Soil hydraulic functions for the different soil layers, expressed through the van Genuchten-  
258 Mualem model, were determined according to the experimental data by using the retention  
259 curve (*RETC*) computer program (van Genuchten et al., 1991). The root distribution parameters  
260 were obtained after calibrating eq. (10) based on the values of normalized *RLD* measured in the  
261 field. The van Genuchten (1987) S-shape model (eq. 7) was adopted to represent the root  
262 water uptake stress function by assuming  $h_{50}=-15,200$  cm and  $p=4.284$ , as estimated by Rallo  
263 and Provenzano (2013) in the same experimental field.

264 Soil water content at the beginning of simulation was supposed constant and equal to  $0.25 \text{ cm}^3$   
265  $\text{cm}^{-3}$  in the whole simulation domain. However, this assumption had a limited effect on soil  
266 water contents and transpiration fluxes measured during irrigation seasons and later used to  
267 validate the model. In fact, after large rainfall events occurring between January and February  
268 2011 the soil reached the field capacity and, as observed in the field, maintained similar  
269 conditions approximately until the end of May.

270 The model was validated according to temporal dynamic of both soil water content and root  
271 water uptake. The latter, under the hypothesis to neglect the tree capacitance, was assumed  
272 corresponding to the dynamic of transpiration fluxes measured with sap flow sensors. The  
273 comparison between measured and simulated soil water contents was carried out in 25 control  
274 points (five different depths of five soil profiles). At each distance and depth from the plant  
275 row, the average *SWC* and the corresponding standard deviation were obtained by considering  
276 the values measured with the *FDR* probe within the installed access tubes. On the other hand,

277 measurements of actual transpiration fluxes were obtained by averaging the daily cumulative  
 278 values acquired by sap flow sensors.

279 Once the model was validated, the relationship between *MSWP* and the ratio between actual  
 280 and maximum tree transpiration, identifying the crop water stress coefficient ( $K_s=T_a/T_m$ ), was  
 281 assessed. Hydrus-2D model allowed then to simulate, under different scenario, the levels of  
 282 crop water stress achieved during the different phases of phenological growth. In particular,  
 283 scenario analysis was carried out to estimate *Ks* and *MSWP* in the absence of irrigation (NI), as  
 284 well as by applying 15%, 30% and 50% of maximum transpiration registered between June 13  
 285 and August 30 of both years, divided in thirteen irrigation events of equal volume applied  
 286 weekly.

287

### 288 *Evaluation of model performance*

289 Hydrus-2D model performance to estimate the spatial and temporal dynamics of soil water  
 290 contents and transpiration fluxes was evaluated based on Mean Bias Error (*MBE*), Root Mean  
 291 Square Error (*RMSE*) and the Efficiency index (*NSE*) proposed by Nash and Sutcliffe, (1970).

$$292 \quad MBE = \frac{\sum_{i=1}^N (X_{obs,i} - X_{sim,i})}{N} \quad (13)$$

$$293 \quad RMSE = \sqrt{\frac{\sum_{i=1}^N (X_{obs,i} - X_{sim,i})^2}{N}} \quad (14)$$

$$294 \quad NSE = 1 - \frac{\sum_{i=1}^N (X_{obs,i} - X_{sim,i})^2}{\sum_{i=1}^N (X_{obs,i} - \bar{X}_{obs})^2} \quad (15)$$

295 where  $X_{obs}$  is the generic value of the considered variable acquired at day *i*,  $X_{sim}$  is the  
 296 corresponding simulated and *N* is the number of measured data.

297 The value of *NSE* can range between  $-\infty \leq NSE \leq 1$ . *NSE* value ranges between 0 and 1 indicates  
 298 that the model is suitable to well reproduce the measured variable, with *NSE*=1 expressive of

299 the perfect agreement, whereas *NSE* values lower than zero identify unacceptable performance  
300 of the model.

301

## 302 **Results and Discussion**

### 303 *Physical characterization of soil and root systems*

304 Table 1 shows the van Genuchten-Mualem parameters of soil water retention and conductivity  
305 functions (eqs. 2-4) obtained for the different investigated soil layers and used for model  
306 simulations. As can be observed, even though quite similar parameters characterized the soil  
307 water retention curves at the different depths, the saturated hydraulic conductivity decreased at  
308 increasing depth from 70 to 20 cm  $d^{-1}$ , due to soil compaction occurring at the higher depths.  
309 Figure 2 shows the normalized root length density (*RLD*) corresponding to the different soil  
310 depths (profiles P1-P13), measured at distances of 0, 50, 100 and 200 cm from the plant row;  
311 the root distribution function obtained after fitting the Vrugt model (eq. 10) to experimental  
312 data is also shown. At each distance from plant row, the mean *RLD* values were initially  
313 determined at the different depths and then used to calibrate the model (eq. 10) according to a  
314 nonlinear Generalized Reduced Gradient (*GRG*) algorithm, by minimizing the variance of  
315 residuals between measured average and estimated *RLD*. The values of parameters, later used  
316 for simulations, resulted respectively equal to  $Z_m = 120$  cm,  $X_m = 580$  cm,  $z^* = 30$  cm,  $x^* = 0$  cm,  
317  $p_z = 1$ ,  $p_x = 2$ .

318 As can be noticed when observing measured data in figure 2, active roots ( $d < 2.0$  mm) exist in  
319 the whole soil domain, even at a certain distance from the tree row along which is installed the  
320 irrigation pipe. For a fixed soil profile, root density tends to decrease at increasing depth,  
321 whereas for a fixed depth with the distance from the plant row; roots are mostly concentrated  
322 in the upper soil layers, till about 40 cm depth. Moreover, closer the soil profile to plant row,

323 more variable *RLD* values, as a consequence of micro irrigation system used for irrigation (drip  
324 lateral along the plant row with four emitters per plant). In fact, the quite high gradients of soil  
325 water content occurring after irrigation events have determined the development of an extended  
326 root system within the wetted soil volume, that justifies the highest (on average) root density  
327 generally detected along the tree row. The achieved results are in agreement with those  
328 observed by Fernandez et al. (1991), who evidenced that under dry conditions, adult olive trees  
329 adapt their roots to the installed drip system, with the highest concentration detected within the  
330 soil volume wetted by emitters. Similarly to what observed by Searles et al. (2009), about 70%  
331 of active roots were found in the soil volume 0.5 m depth and 0.5 m wide, along the drip line.  
332 However, despite a number of papers investigated on root distribution in olive orchards (Rieger,  
333 1995; Moreno et al., 1996; Palese et al., 2000), little information have been provided on the  
334 temporal dynamic of root system distribution (Connor and Fereres, 2005).

335

### 336 ***Model simulations***

337 Figure 3a shows the temporal dynamic of daily precipitation and reference evapotranspiration,  
338 whereas fig. 3b illustrates the temporal patterns of maximum soil evaporation and plant  
339 transpiration occurred during 2011 and 2012, as used to run Hydrus-2D simulations. During  
340 both years, similar climate conditions can be observed, with reference evapotranspiration  
341 ranging between about 1.0 and 6.5 mm d<sup>-1</sup>, and the absence or rainfall during July and August,  
342 during which the highest atmospheric evaporative occurred. Annual reference  
343 evapotranspiration was equal to 1149.3 mm in 2011 and 1153.6 mm in 2012, whereas total  
344 rainfall resulted in the two years of 566.0 and 580.2 mm. The temporal patterns of maximum  
345 evaporation,  $E_m$ , and transpiration,  $T_m$ , (fig. 3b) follow, of course, the dynamic of  $ET_0$ . Annual



346  $T_m$  resulted of 459.7 and 403.6 mm, whereas  $E_m$  was equal to 114.9 and 115.3 mm respectively  
347 in 2011 and 2012.

348 Figure 4 shows the temporal dynamic of measured and simulated soil water contents at different  
349 depths and distances from plant row, as obtained from May to November 2011. At each soil  
350 depth, mean and standard deviation of measured soil water content were obtained by averaging  
351 the values detected in the soil profiles along planes parallels to the plant row. The quite high  
352 standard deviations characterizing all the depths along the plant row (left column of fig. 4) are  
353 due to the high gradient of soil water content consequent to the adopted localized irrigation  
354 system. As it can be observed, Hydrus-2D is in general able to reproduce the trends of measured  
355 soil water contents at the different distances and depths from the plant row, despite simulated  
356 values are referred to the mesh nodes, whereas the corresponding measured are representative  
357 of finite soil volumes. Analogous results were obtained in 2012 in which, however, variability  
358 of measured soil water contents resulted systematically lower than that observed in 2011 (fig.  
359 5). This situation can be related to irrigation system, according to which water was distributed  
360 on the soil surface almost uniformly and thus infiltration process was practically mono-  
361 dimensional. Moreover, overestimations of soil water contents mainly simulated at high depths  
362 and distances from the plant row could be a consequence of the inadequate schematization of  
363 root system, whose distribution was assumed similar to that of 2011. In fact, due to irrigation  
364 system adopted in 2012, the plant could have developed a different root distribution and thus  
365 locally modified root water uptake. The lack of knowledge about the temporal patterns of active  
366 root system, however, does not allow further speculations but the auspice of future  
367 investigations.

368 The temporal dynamic of measured and simulated actual transpiration fluxes, from May 1 to  
369 November 27 of both the examined years, is shown in fig. 6, in which the patterns of maximum

370 transpiration, precipitation and irrigation are also displayed. It can be noticed that simulated  
371 transpiration fluxes in the investigated periods resulted similar to those obtained by integrating,  
372 at daily time-step, sap flow measurements. The local discrepancies, mainly observed around  
373 the end of June and in September 2011, could be due to the neglected tree capacitance and  
374 therefore to the contribute to transpiration fluxes of the water stored in leaves, branches and  
375 trunk of the tree. Table 2 summarizes the results of statistical comparisons between simulated  
376 and measured soil water contents and transpiration fluxes in 2011 and 2012. The best  
377 performance of the model, in terms of both soil water contents and plant transpiration fluxes  
378 was obtained in 2011, as confirmed by the highest values assumed by the Nash-Sutcliffe  
379 efficiency index. However, even in 2012, despite the discussed limitations caused by the  
380 imprecise schematization of root system distribution, *RMSE* values associated to soil water  
381 contents and transpiration fluxes resulted of  $0.09 \text{ cm}^3 \text{ cm}^{-3}$  and  $0.05 \text{ mm}$ , respectively, with *NSE*  
382 index always positive. The achieved results evidences that more appropriate the schematization  
383 of root system, better the model outputs in terms of soil water contents and transpiration fluxes.  
384 Even Phogat et al. (2013), in a study on almond crop, concluded that Hydrus-2D model is able  
385 to reproduce the spatial and temporal dynamic of water content within the soil domain. On the  
386 other hand, for corn crop, Mailhol et al. (2011) stated that the model ability to simulate actual  
387 transpiration fluxes under severe water stress conditions is questionable. It is necessary to stress  
388 in fact, that in the investigated silty-clay-loam soil, the root system occupies approximately the  
389 whole soil domain. Under these conditions, plant can modify its capability to uptake water from  
390 soil, by activating roots located in soil regions where water is more easily available. This  
391 situation has been observed when examining the variations of soil water contents in the different  
392 regions of root domain after an irrigation or a rainfall event. In the former, according to root  
393 distribution and to drip irrigation system, water uptake occurred mainly from a parallelepiped

394 soil volume having width, length and depth respectively of about 1.50, 5.00 and 0.75 m,  
395 whereas in the latter root water uptake took place from all the root domain (data not shown).  
396 The relatively limited soil water contents measured in 2012 at higher distances from plant row  
397 and deeper soil layers, associated to the relatively high values of actual evapotranspiration  
398 (practically equal to maximum), confirms the root system adaptation capabilities to restrictive  
399 soil water status.

400 Figure 7 shows the absolute values of *MSWP* measured in 2011 as a function of relative  
401 transpiration, calculated as the ratio between simulated actual and maximum crop transpiration  
402 ( $K_s = T_a/T_m$ ). As can be observed the two variables are strongly correlated, being the trend of  
403 *MSWP* (absolute value) decreasing at increasing  $K_s$ . In particular, according to experimental  
404 data and simulation results, a value of  $MSWP = -1.5$  MPa brings to actual transpiration of about  
405 86% of maximum, whereas  $MSWP = -3.1$  MPa determines actual transpiration of 50% of the  
406 corresponding maximum. Rallo et al. (2017), even for citrus crop, identified the relationship  
407 between *MSWPs* and crop water stress coefficients simulated by FAO-56 model, later used to  
408 assess the linear correlations existing between measured and simulated water stress integrated  
409 over the season, which was dependent on the adopted irrigation strategy. According to the  
410 performed analysis then, it is possible to conclude that Hydrus-2D model, under the examined  
411 conditions, is also suitable to identify the variability of crop water status.

412 The model was finally used to simulate the levels of crop water stress achieved in the different  
413 phenological phases. Table 3 summarizes the values of cumulative precipitation, irrigation,  
414 maximum and actual transpiration registered in 2011 and 2012, between June 13 and August  
415 30, as well as average ( $\mu$ ) and standard deviation ( $\sigma$ ) of *MSWP* in the different stages of  
416 vegetative growth occurring in the period. On the other hand, fig. 8a,b illustrates the temporal  
417 dynamic of maximum and actual transpiration, whereas fig. 8c,d shows the corresponding crop

418 water stress coefficient, obtained respectively in 2011 and 2012 under the examined scenarios.  
419 At the beginning of both years actual transpiration simulated in all the examined scenarios  
420 resulted equal to the maximum, as a consequence of soil water status that did not result limiting  
421 crop transpiration. Then, as expected, actual transpiration decreased more and more rapidly at  
422 decreasing irrigation depths, being the minimum values achieved in the absence of irrigation  
423 (NI). The values of relative transpiration, ranging approximately between 0.3 and 1.0, reached  
424 the minimum around the begin of October in 2011 and at the end of August in 2012.

425 Based on the empirical relationship between midday stem water potential and  $K_s$  obtained for  
426 the examined site (fig. 7), the temporal dynamic of  $MSWP$  was also determined for the two  
427 years and under the different irrigation scheduling scenarios, as shown respectively in fig. 8e,f.  
428 Horizontal lines specifies the thresholds for mild (-2.0 MPa) and moderate (-3.5 MPa) water  
429 stress levels as obtained over four growing season by Ahumada-Orellana et al. (2017) in a  
430 super-high density olive orchards. The results of these Authors evidenced in particular, that  
431 reducing  $MSWP$  till reaching the threshold of -3.5 MPa during pit hardening has not significant  
432 effects on crop yield and determines a reduction of about 20% of seasonal irrigation. The  
433 reduction of irrigation during pit hardening, generally characterized by high atmospheric  
434 evaporative demands, has been suggested by many authors as suitable  $RDI$  strategy for the  
435 examined crop, because this phase of vegetative growth is the least sensitive to water deficit  
436 (Goldhamer, 1999). However, it has to be considered that the optimal  $MSWP$  may be different  
437 according to soil physical characteristics or with climate variables, such as vapour pressure  
438 deficit and air temperature (Corell et al., 2016). Under the examined scenarios, whilst  
439 maintaining the olive trees under rainfed conditions may bring to severe crop water stress during  
440 stage II of fruit growth with consequent reductions of crop yield, the scenario  $S_{50}$ , obtained by  
441 scheduling irrigation of the period between June 13 and August 30 as 50% of maximum

442 transpiration, allows maintaining *MSWP* always below the threshold of mild water stress.  
443 However, independently from the chosen thresholds, a physically based model such as Hydrus-  
444 2D can represent a powerful tool to improve irrigation strategies under water constraints, also  
445 accounting for economic considerations.

446

## 447 **Conclusion**

448 The knowledge of actual *ET* fluxes and crop water status has a significant role in regions where  
449 water resources for agriculture are limited and deficit irrigation is practiced as water  
450 management strategy. This study examined the performance of Hydrus-2D numerical model to  
451 predict soil water contents and transpiration fluxes in an olive orchard irrigated with two  
452 different irrigation systems. Additional measurements of midday stem water potential (*MSWP*)  
453 allowed calibrating the relationship occurring with the relative transpiration simulated by the  
454 model. A scenario analysis was finally carried out in order to verify the possibility to decrease  
455 the seasonal irrigation water requirement by controlling the levels of crop water stress achieved  
456 by crop in the different phases of vegetative growth.

457 The analysis demonstrates that the patterns of soil water contents reproduced by the model were  
458 comparable to the corresponding measured at the experimental site, with *RMSE* values of 0.04  
459 and 0.09 cm<sup>3</sup> cm<sup>-3</sup> in 2011 and 2012, respectively. Moreover, ~~when the model is adequately~~  
460 ~~calibrated and the root system correctly schematized,~~ Hydrus-2D it is able to reproduce the  
461 temporal dynamic of actual daily transpiration, with *RMSE* values of 0.09 and 0.05 mm in the  
462 examined years and with *NSE* index always positive. The obtained results evidenced that more  
463 appropriate the schematization of root system, better the model outputs in terms of soil water  
464 contents and transpiration fluxes.

465 With respect to scenario analysis, it was verified that under the examined conditions the absence  
466 of irrigation may bring to severe stress in periods when the crop is sensitive to water deficit  
467 (stage II of vegetative growth). On the other hand, the application of volumes equal to 50% of  
468 maximum transpiration in the period from June 13 to August 30, allows maintaining *MSWP*  
469 always below the threshold of mild water stress. Hence, independently from the thresholds  
470 chosen to describe the levels of crop water stress, a physically based model such as Hydrus-2D  
471 can represent a powerful tool in evaluating the impact of deficit irrigation and improving water  
472 saving strategies under water constraints. We believe that information obtained in this study  
473 can be utilized for developing better management practices for olive orchards.  
474 Further investigations, however, have to consider the effects of tree capacitance on transpiration  
475 fluxes, as well as how irrigation systems can affect the patterns of active roots and the dynamic  
476 of water uptake.

477

## 478 **References**

- 479 Allen, R.G., Pereira, L.S., Raes, D., Smith, M. 1998. Crop evapotranspiration. Guideline for  
480 computing crop water requirements. FAO irrigation and drainage paper n. 56, Rome,  
481 Italy, 326 pp.
- 482 Allen, R.G., Pereira, L.S. 2009. Estimating crop coefficients from fraction of ground cover and  
483 height. *Irrigation Science* 28, 17-34. DOI:10.1007/s00271-009-0182-z.
- 484 Ahumada-Orellana, L.E., Ortega-Farías, S., Searles, P.S., Retamales, J.B. 2017. Yield and  
485 water productivity responses to irrigation cut-off strategies after fruit set using stem water  
486 potential thresholds in a super-high density olive orchard. *Frontiers in Plant Science*, 8,  
487 article 1280. DOI: 10.3389/fpls.2017.01280.
- 488 Autovino, D., Provenzano, G., Monserrat, J., Cots, L., Barragán, J. 2016. Determining optimal  
489 seasonal irrigation depth based on field irrigation uniformity and economic evaluations:  
490 Application for onion crop. *Journal of Irrigation and Drainage Engineering* 142(10). DOI:  
491 10.1061/(ASCE)IR.1943-4774.0001048.

492 Bagarello, V., Di Prima, S., Iovino, M., Provenzano, G., Sgroi, A. 2011. Testing different  
493 approaches to characterize Burundian soils by the BEST procedure. *Geoderma* 162(1-2),  
494 141-150. DOI: 10.1016/j.geoderma.2011.01.014.

495 Burke, W., Gabriels, D., Bouma, J. 1986. *Soil Structure Assessment*. Balkema, Rotterdam, The  
496 Netherlands.

497 Cammalleri, C., Rallo, G., Agnese, C., Ciruolo, G., Minacapilli, M., Provenzano, G. 2013.  
498 Combined use of eddy covariance and sap flow techniques for partition of ET fluxes and  
499 water stress assessment in an irrigated olive orchard. *Agricultural Water Management*,  
500 120, 89-97. DOI: org/10.1016/j.agwat.2012.10.003.

501 Celia, M.A., Bouloutas, E.T., Zarba, R.L. 1990. A general mass conservative numerical  
502 solution for the unsaturated flow equation. *Water Resources Research* 26, 1483-1496.

503 Connor, D.J., Fereres, E., 2005. The physiology of adaptation and yield expression in olive.  
504 *Hortic. Rev.* 31, 155–229.

505 Corell, M., Pérez-López, D., Martín-Palomo, M. J., Centeno, A., Girón, I., Galindo, A., et al.  
506 (2016). Comparison of the water potential baseline in different locations. Usefulness for  
507 irrigation scheduling of olive orchards. *Agricultural Water Management*, 177, 308-316.  
508 doi: 10.1016/j.agwat.2016.08.017.

509 Dane, J.H., Hopman, J.W. 2002. Water retention and storage. In: Dane, J.H., Topp, G.C. (Eds.),  
510 *Methods of Soil Analysis: Part 4-Physical methods*. SSSA Book Ser. 5. SSSA, Madison.

511 Egea, G., Diaz-Espejo, A., Fernández, J.E. 2016. Soil moisture dynamics in a hedgerow olive  
512 orchard under well-watered and deficit irrigation regimes: Assessment, prediction and  
513 scenario analysis. *Agricultural Water Management* 164, 197-211. DOI:  
514 10.1016/j.agwat.2015.10.034.

515 Feddes, R.A., Kowalik, P.J., Zaradny, H. 1978. *Simulation of field water use and crop yield*.  
516 Pudoc, Centre Agric. Publ. Doc., Wageningen, The Netherland.

517 Fernandez, J.E., Moreno, F., Cabrera, J.L., Arrue, J.L., Martin-Aranda, J., 1991 - Drip  
518 irrigation, soil characteristics and the root distribution and root activity of olive trees.  
519 *Plant and Soil*, 133, 239-251.

520 Gamon, J. A., Qiu, H. 1999. Ecological applications of remote sensing at multiple scales. In F.  
521 I. Pugnaire, & F. Valladares (Eds.), *Handbook of functional plant ecology*. New York:  
522 Marcel Dekker, Inc.

523 Ghazouani, H., Autovino, D., Rallo, G., Douh, B., Provenzano, G. 2016. Using Hydrus-2D  
524 model to assess the optimal drip lateral depth for Eggplant crop in a sandy loam soil of  
525 central Tunisia. *Italian Journal of Agrometeorology* 1, 47-58. DOI:  
526 10.19199/2016.1.2038-5625.047.

527 Goldhamer, D.A. 1999. Regulated deficit irrigation for California canning olives. *Acta Hort.*  
528 474, 369–372. doi: 10.17660/ActaHortic.1999.474.76.

529 Granier, A. 1987. Evaluation of transpiration in a Douglas-fir stand by means of sap flow  
530 measurements. *Tree Physiology* 3, 309-320.

531 Homae, M. 1999. Root water uptake under non-uniform transient salinity and water stress.  
532 Ph.D. dissertation. Wageningen Agric. Univ., Wageningen, The Netherlands, 173 pp.

533 Jones, H.G. 2004. Irrigation scheduling: advantages and pitfalls of plant-based methods  
534 *Journal of Experimental Botany*, Volume 55, Issue 407, 1 November 2004, Pages 2427–  
535 2436,

536 Kramer, P.J. 1969. *Plant and soil water relationships*. Mc-Graw-Hill Book Co., New York.

537 Logsdon, S.D., Radke, J.K., Karlen, D.L. 1993. Comparison of alternative farming systems. I.  
538 Infiltration techniques. *American Journal of Alternate Agriculture* 8(1), 15-20. DOI:  
539 10.1017/S0889189300004860.

540 Mailhol J.C., Ruelle, P., Walser, S., Schütze, N., Dejean, C. 2011. Analysis of AET and yield  
541 predictions under surface and buried drip irrigation systems using the Crop Model  
542 PILOTE and Hydrus-2D. *Agricultural Water Management*, 98, 1033-1044.  
543 doi:10.1016/j.agwat.2011.01.014.

544 Martí, P., Provenzano, G., Royuela, T., Palau-Salvador, G. 2010. Integrated emitter local loss  
545 prediction using artificial neural networks. *Journal of Irrigation and Drainage*  
546 *Engineering* 136(1), 11-22. DOI: 10.1061/(ASCE)IR.1943-4774.0000125.

547 Mguidiche, A., Provenzano, G., Douh, B., Khila, S., Rallo, G., Boujelben, A. 2015. Assessing  
548 Hydrus-2D model to simulate water content and salt accumulation in a soil irrigated with  
549 a subsurface drip system: Application in a semiarid area of central Tunisia. *Irrigation and*  
550 *Drainage* 64(2), 263-274. DOI: 10.1002/ird.1884.

551 Minacapilli, M., Agnese, C., Blanda, F., Cammalleri, C., Ciraolo, G., D’Urso, G., Iovino, M.,  
552 Pumo, D., Provenzano, G., Rallo, G. 2009. Estimation of actual evapotranspiration of  
553 Mediterranean perennial crops by means of remote-sensing based surface energy balance  
554 models. *Hydrology and Earth Science System* 13(7), 1061-1074.



555 Minacapilli, M., Cammalleri, C., Ciraolo, G., Rallo, G., Provenzano, G. 2016. Using  
556 scintillometry to assess reference evapotranspiration methods and their impact on the  
557 water balance of olive groves. *Agricultural Water Management* 170, 49-60. DOI:  
558 10.1016/j.agwat.2015.12.004.

559 Moreno, F., Fernández, J.E., Clothier, B.E., Green, S.R. 1996. Transpiration and root water  
560 uptake by olive trees. *Plant Soil* 184, 85-96.

561 Mualem, Y., 1976. A new model for predicting the hydraulic conductivity of unsaturated porous  
562 media. *Water Resources Research* 12, 513-522.

563 Nash J.E., Sutcliffe J.V. 1970. River flow forecasting through conceptual models: Part 1. A  
564 discussion of principles. *Journal of Hydrology* 10(3), 282-290.

565 Newman, E.I., 1966. A method of estimating the total length of root in a sample. *Journal of*  
566 *Applied Ecology* 3, 139-145.

567 Palese, A.M., Nuzzo V., Dichio B., Celano G., Romano M., Xiloyannis C., Ferreira, M.I., Jones,  
568 H.G. 2000. The influence of soil water content on root density in young olive trees. *Acta*  
569 *Hort.* 537, 329-336.

570 Phogat, V., Skewes, M.A., Mahadevan, M., Cox, J.W. 2013. Evaluation of soil plant system  
571 response to pulsed drip irrigation of an almond tree under sustained stress conditions.  
572 *Agricultural Water Management* 118, 1-11. DOI: 10.1016/j.agwat.2012.11.015

573 Provenzano, G., Rodriguez-Sinobas, L. 2014. Special issue on trends and challenges of  
574 sustainable irrigated agriculture. *Journal of Irrigation and Drainage Engineering* 140(9),  
575 DOI: 10.1061/(ASCE)IR.1943-4774.0000773.

576 Provenzano, G., Rodriguez-Sinobas, L., Roldán-Cañas, J. 2014. Irrigated agriculture: Water  
577 resources management for a sustainable environment. *Biosystems Engineering* 128, 1-3.  
578 DOI: 10.1016/j.biosystemseng.2014.10.008.

579 Provenzano, G., Rallo, G., Ghazouani, H. 2015. Assessing field and laboratory calibration  
580 protocols for the Diviner 2000 probe in a range of soils with different textures. *Journal of*  
581 *Irrigation and Drainage Engineering* 142(2). DOI: 10.1061/(ASCE)IR.1943-  
582 4774.0000950.

583 Rallo, G., Provenzano, G. 2013. Modelling eco-physiological response of table olive trees  
584 (*Olea Europea L.*) to water stress. *Agricultural Water Management* 120, 79-88. DOI:  
585 org/10.1016/j.agwat.2012.10.005.

- 586 Rallo, G., Provenzano, G. 2014. Discussion of "Laboratory and Field Calibration of the Diviner  
587 2000 Probe in Two Types of Soil, by J. Haberland, R. Gálvez, C. Kremer, and C. Carter."  
588 Journal of Irrigation and Drainage Engineering 141(8). DOI: 310.1061/(ASCE)IR.1943-  
589 4774.0000856.
- 590 Rallo, G., Agnese, C., Blanda, F., Minacapilli, M., Provenzano, G. 2010. Agro-Hydrological  
591 models to schedule irrigation of Mediterranean tree crops. Italian Journal of  
592 Agrometeorology (1), 11-21.
- 593 Rallo, G., Agnese, C., Minacapilli, M., Provenzano, G. 2012. Comparison of SWAP and FAO  
594 Agro-Hydrological Models to Schedule Irrigation of Wine Grape. Journal of Irrigation  
595 and Drainage Engineering 138(1). DOI: 10.1061/(ASCE)IR.1943-4774.0000435.
- 596 Rallo, G., Baiamonte, G., Manzano, J., Provenzano, G., 2014a. Improvement of FAO-56 model  
597 to estimate transpiration fluxes of drought tolerant crops undersoil water deficit:  
598 application for olive groves. Journal of Irrigation and Drainage Engineering 140(9). DOI:  
599 10.1061/(ASCE)IR.1943-4774.0000693.
- 600 Rallo, G., Minacapilli, M., Ciraolo, G., Provenzano, G. 2014b. Detecting crop water status in  
601 mature olive groves using vegetation spectral measurements. Biosystems Engineering  
602 128, 52-68. DOI: 10.1016/j.biosystemseng.2014.08.012.
- 603 Rallo, G., González-Altozano, P., Manzano-Juárez, J., Provenzano, G. 2017. Using field  
604 measurements and FAO-56 model to assess the eco-physiological response of citrus  
605 orchards under regulated deficit irrigation. Agricultural Water Management 180, 136-  
606 147. DOI: 10.1016/j.agwat.2016.11.011.
- 607 Rieger, M. 1995. Offsetting effects of reduced root hydraulic conductivity and osmotic  
608 adjustment following drought. Tree Physiol. 15, 379-385.
- 609 Scholander, R.R., Hammel, H.T., Bradstreet, E.D., Hemmielsen, E.A. 1965. Sap pressure in  
610 vascular plants. Science 148, 339-346.
- 611 Searles, P.S., Saravia, D.A., Rousseaux, M.C. 2009. Root length density and soil water  
612 distribution in drip-irrigated olive orchards in Argentina under arid conditions. Crop  
613 Pasture Sci., 60, 280-288. <https://doi.org/10.1071/CP08135>
- 614 Šimůnek J., Šejna M., van Genuchten M.Th. 1999. The Hydrus-2D software package for  
615 simulating two-dimensional movement of water, heat, and multiple solutes in variably  
616 saturated media. Version 2.0, IGWMC - TPS - 53, International Ground Water Modeling  
617 Center, Colorado School of Mines, Golden, Colorado, 251pp.+

618 Šimůnek, J., van Genuchten, M.Th., Šejna, M. 2012. Hydrus: Model use, calibration and  
619 validation. *Transaction of the ASABE* 55(4), 1261-1274. DOI: 10.13031/2013.42239.

620 Šimůnek, J., Šejna, M., van Genuchten, M.Th. 2016. Recent Developments and Applications of  
621 the Hydrus Computer Software Packages. *Vadose Zone Journal*, 1-25. DOI:  
622 10.2136/vzj2016.04.0033.

623 Skaggs, T.H., Trout, T.J., Rothfuss, Y. 2010. Drip irrigation water distribution pattern: Effects  
624 of emitter rate, pulsing and antecedent water. *Soil Science Society of America Journal*  
625 74, 1886-1896. DOI: 10.2136/sssaj2009.0341.

626 Tognetti, R., D'Andria, R., Morelli, G., Calandrelli, D., Fragnito, F. 2004. Irrigation effects on  
627 daily and seasonal variations of trunk sap flow and leaf water relations in olive trees. *Plant*  
628 *and Soil* 263(1-2), 249-264. DOI: 10.1023/B:PLSO.0000047738.96931.91.

629 Turner, M.T., Jarvis, G.P. 1982. Measurement of plant water status by the pressure chamber  
630 technique. *Irrigation Science* 9, 289-308.

631 van Genuchten, M.Th. 1980. A closed form equation for predicting the hydraulic conductivity  
632 of unsaturated soils. *Soil Science Society of America Journal* 44, 892-898.

633 van Genuchten, M. Th. 1987. A numerical model for water and solute movement in and below  
634 the root zone. Research Report No 121, U.S. Salinity laboratory, USDA, ARS, Riverside,  
635 California, 221 pp.

636 van Genuchten, M.T., Leij, F.J., Yates, S.R. 1991. The RETC code for quantifying the hydraulic  
637 functions of unsaturated soils. Version 6.02. EPA Report 600/2-91/065, Riverside,  
638 California, 93 pp.

639 Vogel, T. 1987. SWMII - Numerical model of two-dimensional flow in a variably saturated  
640 porous medium, Research Report no. 87, Dept. of Hydraulics and Catchment Hydrology,  
641 Agricultural University, Wageningen, The Netherlands.

642 Vrugt J.A., Hopmans J.W., Šimůnek J. 2001. Calibration of a two-dimensional root water  
643 uptake model. *Soil Science Society of America Journal* 65(4), 1027-1037.

644

645

646

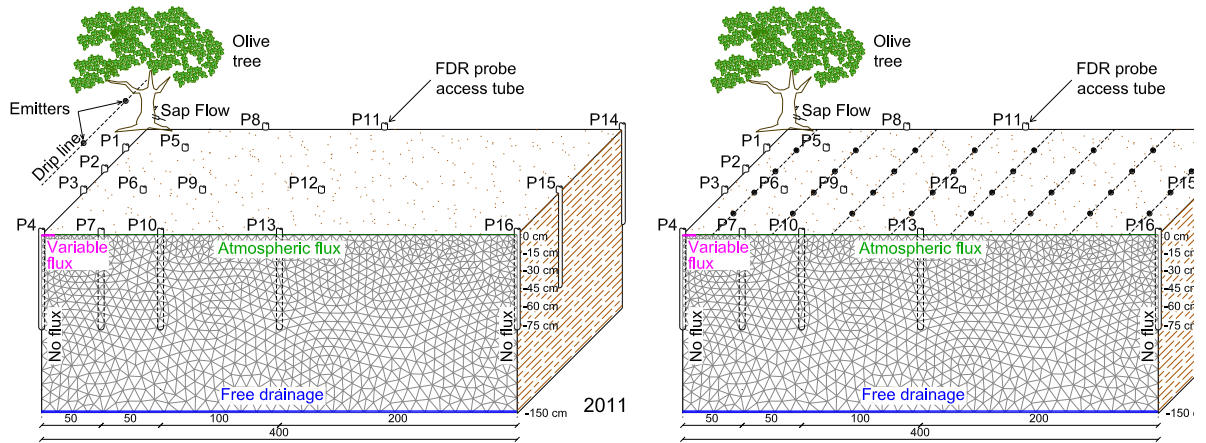


Figure 1a, b - Schematization of simulation domains, positions of FDR probe access tubes and layout of irrigation systems used in 2011 (a) and 2012 (b)

647

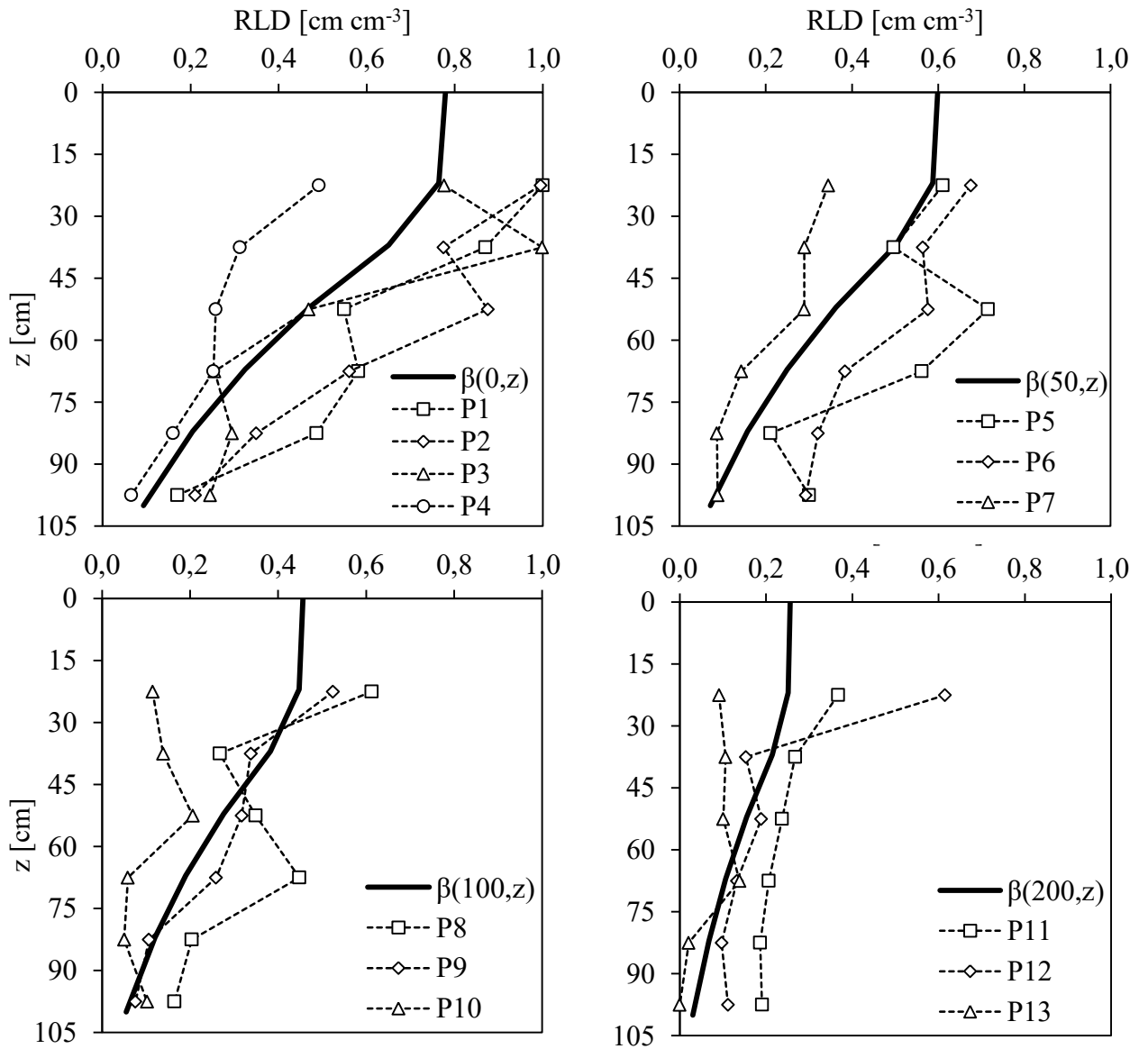


Figure 2 – Profiles of normalized root length density, *RLD*, measured in P1-P13, at distances of 0, 50, 100 and 200 cm from the plant row. *RLD* profiles, according to the Vrugt model at each distance are also shown.



651

652

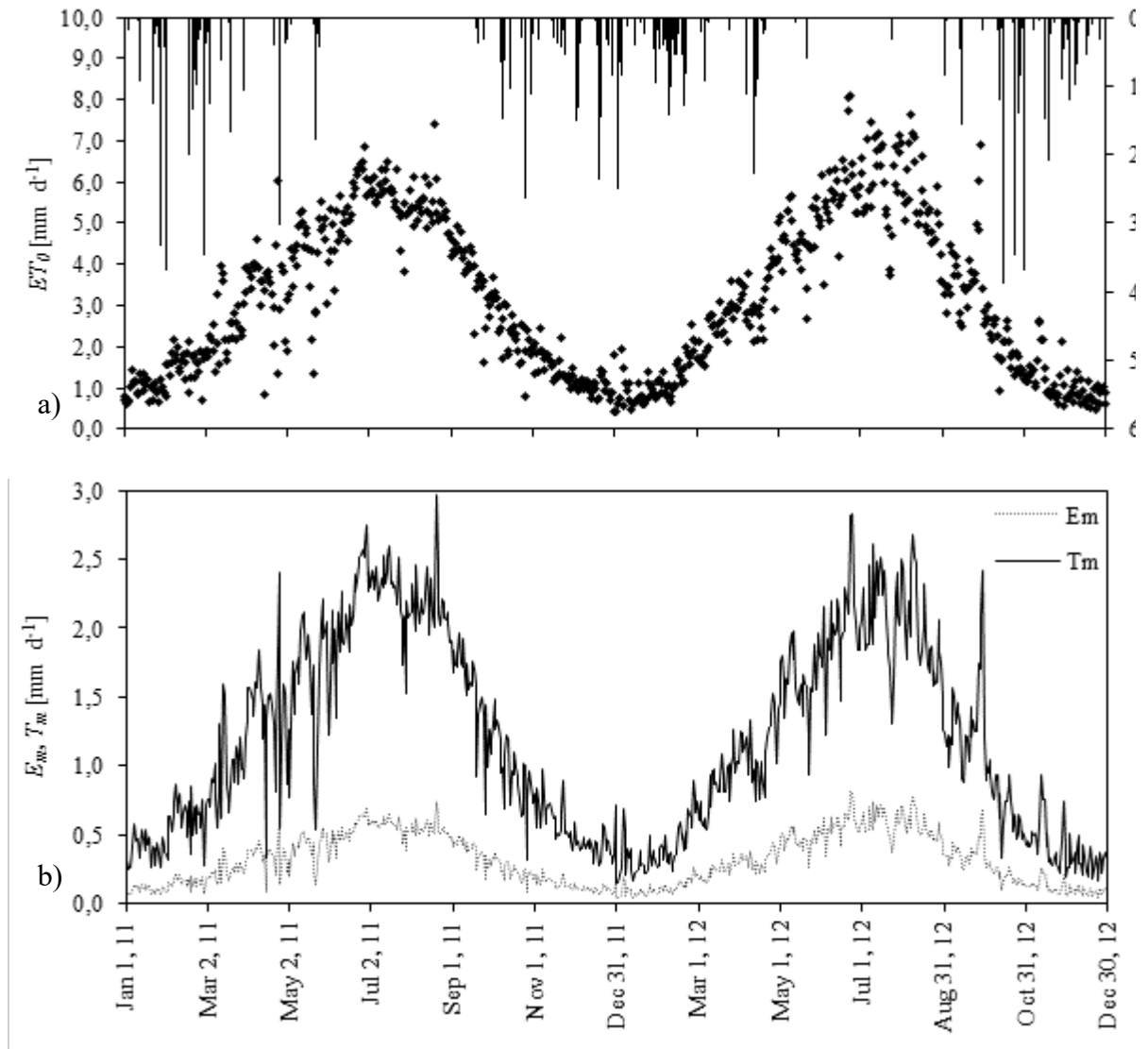


Figure 3a, b - a) Temporal dynamic of reference evapotranspiration,  $ET_0$  and precipitation,  $P$ , and b) maximum soil evaporation,  $E_m$ , and plant transpiration,  $T_m$ , estimated in 2011 and 2012

653

654

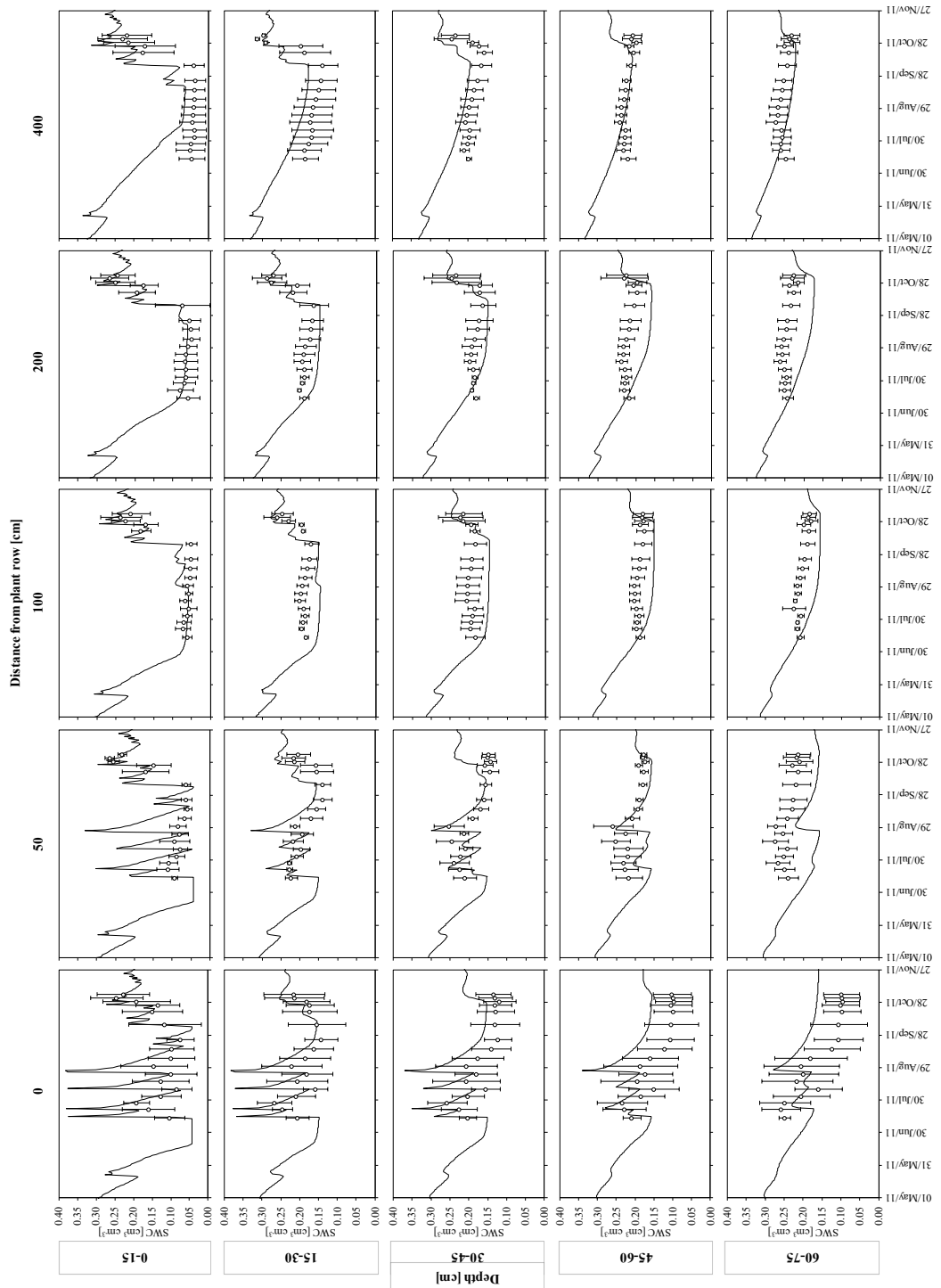


Figure 4 - Temporal dynamic of measured and simulated soil water contents at different depths and distances from the plant row, as obtained in the period May 1 - November 27, 2011



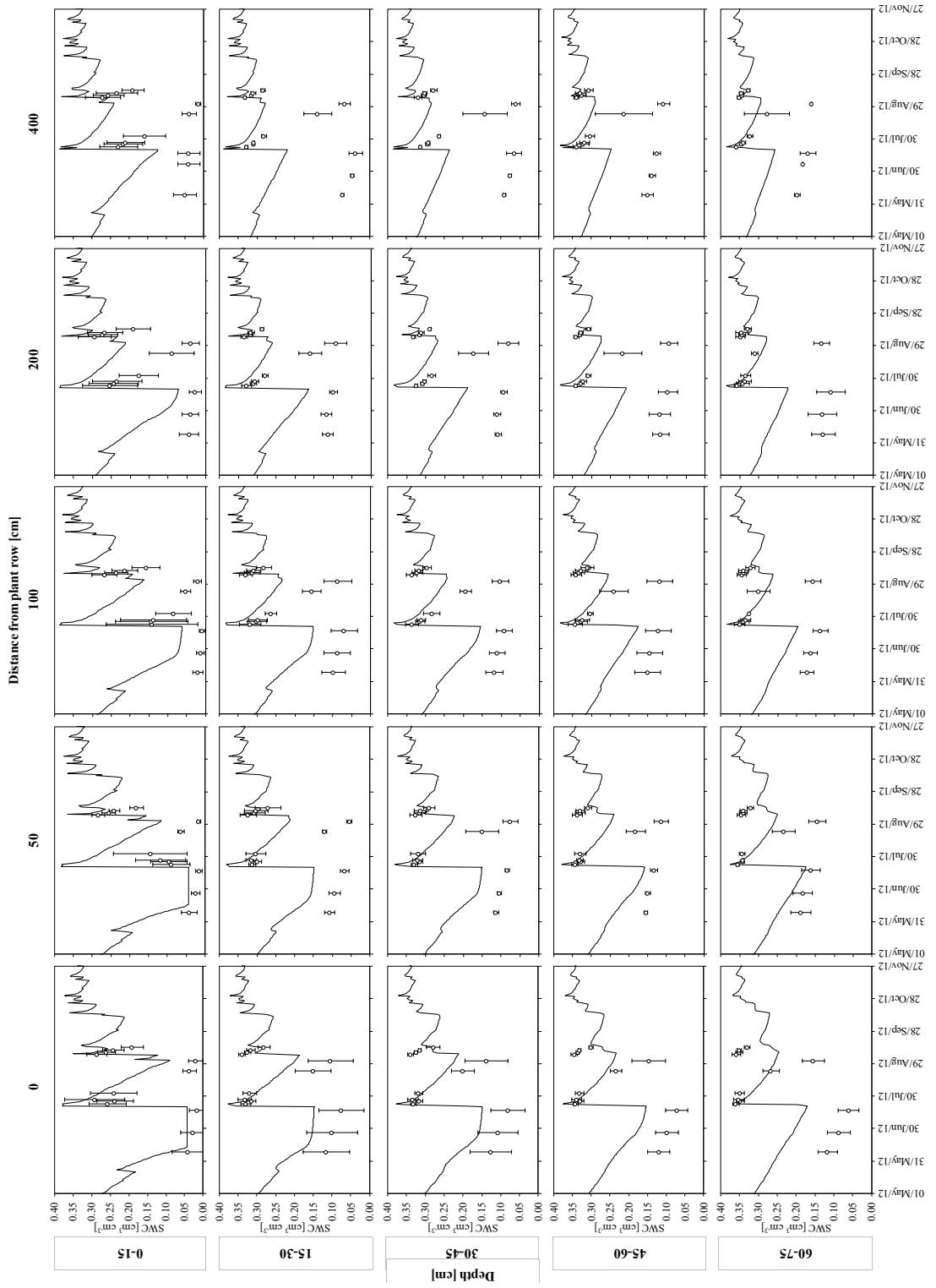


Figure 5 - Temporal dynamic of measured and simulated soil water contents at different depths and distances from the plant row, as obtained in the period May 1 - November 27, 2012

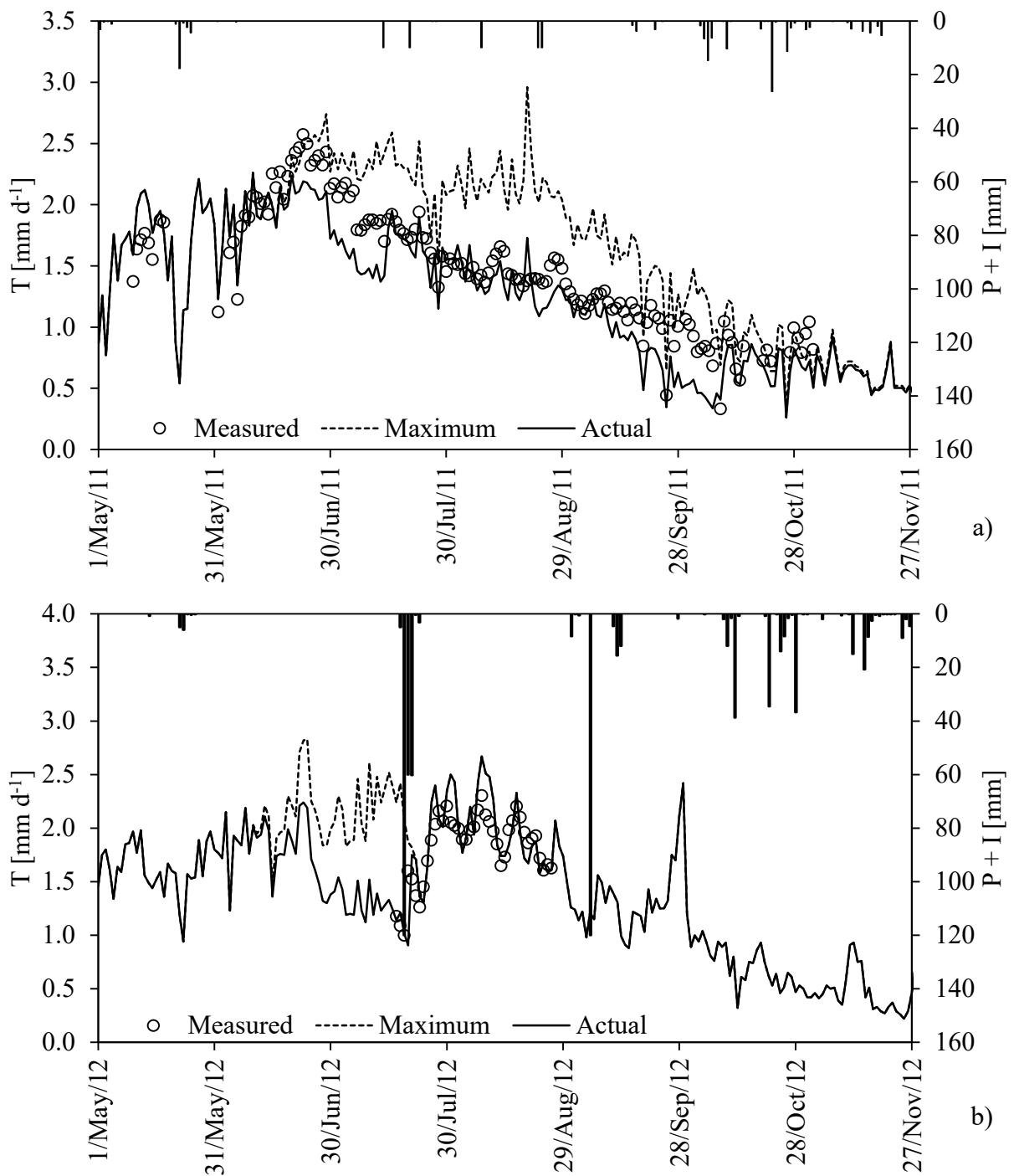


Figure 6a, b - Temporal dynamic of measured and simulated actual transpiration.  $T_a$ , from May 1 to November 27, 2011 (a) and 2012 (b). The patterns of maximum transpiration,  $T_m$ , precipitation,  $P$ , and irrigation,  $I$ , are also shown.

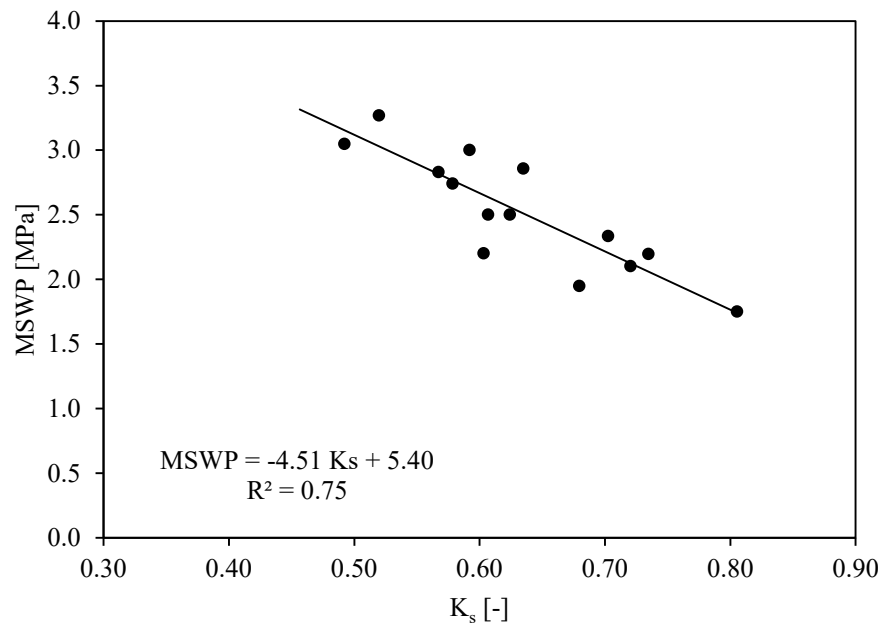


Figure 7 - Midday Stem Water Potential (MSWP) versus estimated stress coefficient ( $K_s=T_a/T_m$ )

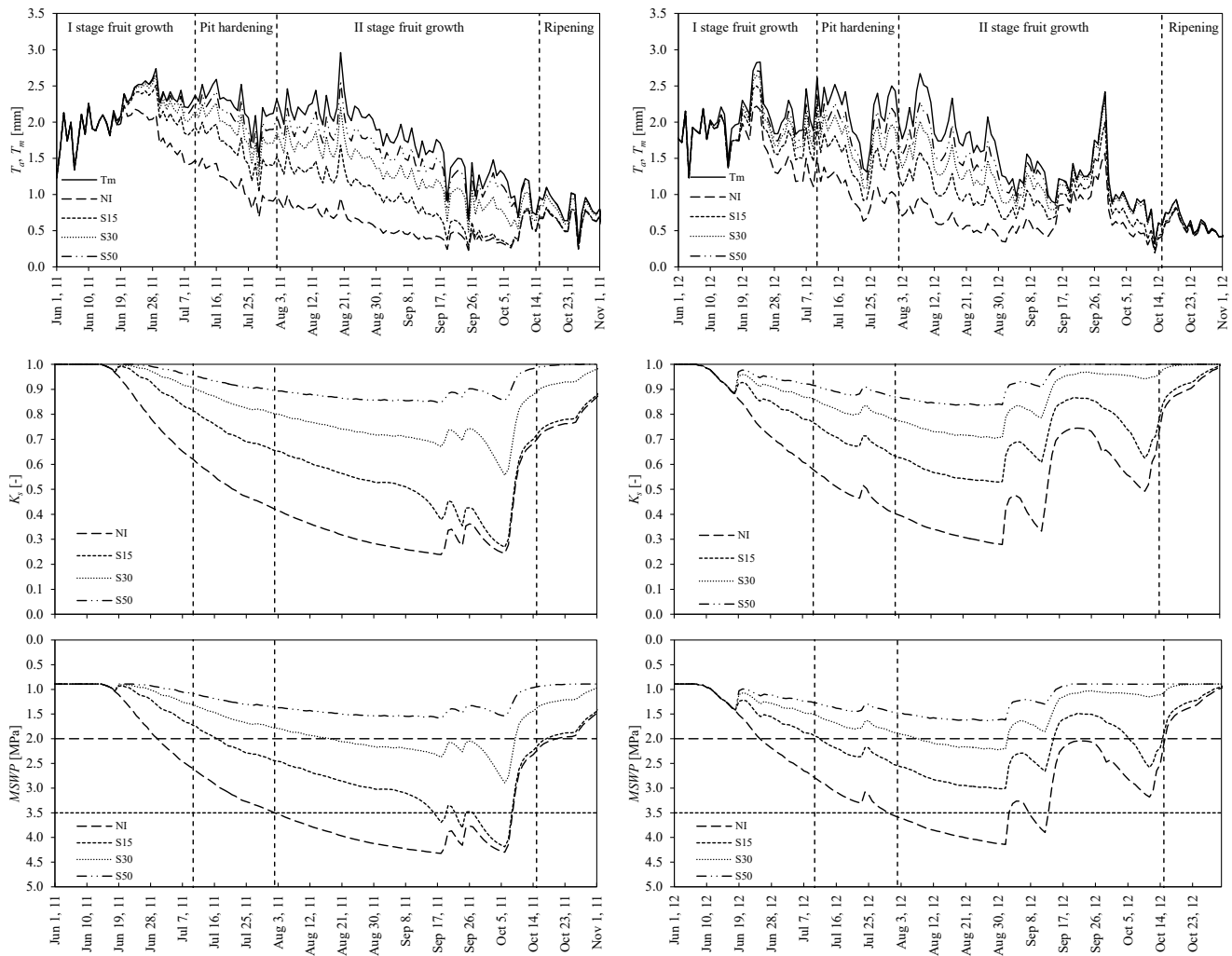


Figure 8 – Temporal dynamic of maximum and simulated actual transpiration (a, b), crop water stress coefficient (c, d) and Midday Stem Water Potential (e, f) under different irrigation scheduling scenarios, as obtained in 2011 and 2012. Horizontal lines in the lower graphs represents the thresholds of mild (2.0 MPa) and moderate (3.5 MPa) stress.

655

656

657

658

659

660

661

662

663  
664  
665  
666  
667  
668

Depth [cm]	$\theta_s$ [cm <sup>3</sup> cm <sup>-3</sup> ]	$\theta_r$ [cm <sup>3</sup> cm <sup>-3</sup> ]	$\alpha$ [-]	$n$ [-]	$K_s$ [cm d <sup>-1</sup> ]	$\lambda$ [-]
0-15	0.39	0.00	0.008	1.32	70	0.5
15-45	0.39	0.06	0.014	1.21	60	0.5
50-70	0.39	0.06	0.014	1.21	40	0.5
80-100	0.39	0.06	0.022	1.18	20	0.5

Table 1 - Parameters of soil hydraulic functions.

Year	Soil Water Contents				Transpiration Fluxes			
	$N$	$MBE$ [cm <sup>3</sup> cm <sup>-3</sup> ]	$RMSE$ [cm <sup>3</sup> cm <sup>-3</sup> ]	$NSE$ [-]	$N$	$MBE$ [mm]	$RMSE$ [mm]	$NSE$ [-]
2011	400	-0.004	0.04	0.51	152	-0.16	0.09	0.61
2012	400	-0.056	0.09	0.18	41	0.06	0.05	0.44

669  
670  
671  
672

Table 2 – Results of statistical analysis carried out to compare simulated and measured soil water contents and transpiration fluxes in 2011 and 2012 ( $N$ = number of observations).

	Climate variables					MSWP Pit hardening					
	P	I	$T_m$ [mm]	$T_a$	D	I Stage		II Stage		II Stage	
						$\mu$	$\sigma$	$\mu$	$\sigma$	$\mu$	$\sigma$
2011											
NI		0.0		87.9	2.1	1.4	0.6	3.1	0.3	3.9	0.5
S <sub>15</sub>	0.4	25.0	166.6	121.6	2.0	1.1	0.3	2.1	0.2	3.1	0.5
S <sub>30</sub>		50.0		141.3	2.1	1.0	0.1	1.6	0.1	2.1	0.3
S <sub>50</sub>		83.3		153.7	5.1	0.9	0.1	1.2	0.1	1.4	0.1
2012											
NI		0.0		76.1	1.6	1.7	0.7	3.2	0.2	3.3	0.7
S <sub>15</sub>	3.8	22.9	152.4	105.7	1.6	1.3	0.3	2.3	0.2	2.4	0.5
S <sub>30</sub>		45.7		123.9	1.6	1.2	0.2	1.7	0.1	1.6	0.5
S <sub>50</sub>		76.2		135.8	2.9	1.1	0.1	1.4	0.1	1.2	0.3

673  
674  
675  
676

Table 3 – Values of precipitation, irrigation, maximum and actual transpiration registered in 2011 and 2012, between June 13 and August 30. Average ( $\mu$ ) and standard deviation ( $\sigma$ ) of MSWP in the different stages of vegetative growth are also indicated.